

RESEARCH PAPER

Optimization of microwave irradiation time for KOH-activated carbon from oil palm fronds

Rahmt Zikri*[a], Ayu Sapitri[b] and Yolanda Rati [c]

- [a] Department of Chemistry Education, Faculty of Teacher Training and Education, Sriwijaya University, Palembang, Indonesia
- [b] Department of Chemistry, Faculty of Mathematics and Natural Sciences, Riau University, Pekanbaru, Indonesia
- [c] Department of Physics, Faculty of Mathematics and Natural Sciences, Sumatera Institute of Technology, Lampung, Indonesia

*E-mail: rahmatzikri@fkip.unsri.ac.id

DOI: 10.29303/aca.v8i2.275

Article info:

Received 07/10/2025

Revised 02/11/2025

Accepted 10/11/2025

Available online 29/11/2025

Abstract: Activated carbon is a widely applied adsorbent material in wastewater treatment, whose physical and chemical properties are strongly influenced by the activation method employed. Microwave irradiation-based physical activation has emerged as an attractive alternative, offering shorter processing times and lower energy consumption compared to conventional heating methods. This study aims to evaluate the effect of varying microwave irradiation times on the characteristics of activated carbon derived from oil palm fronds (OPF) waste. The synthesis process began with carbonization at 600 °C for 60 minutes to produce OPF char, followed by chemical activation using KOH with a char-to-KOH mass ratio of 1:1 (g/g) in 100 mL of demineralized water, and subsequently physical activation using a microwave at 200 W for 5 minutes (A5D200), 10 minutes (A10D200), and 15 minutes (A15D200). Characterization was conducted in accordance with SNI 06-3730-1995 standards (moisture content, ash content, and iodine adsorption capacity), as well as physicochemical analyses including crystallinity, surface area, functional groups, morphology, and elemental composition. The results demonstrated that all samples met the SNI requirements, with the highest iodine adsorption capacity (828.69 mg/g) and the largest surface area (824.26 m²/g) obtained at A10D200. XRD analysis revealed the dominance of amorphous structures with an increasing Lc/La ratio as the irradiation time increased, while SEM images showed relatively small and uniformly distributed pores. FTIR spectra confirmed the presence of O-H, C=O, C=C, C-H, and C-O functional groups. In conclusion, a 10minute irradiation time produced activated carbon with an optimal balance between pore structure, surface area, and adsorption capacity.

Keywords: Activated Carbon, Microwave, Oil Palm Fronds.

Citation: Zikri, R., Sapitri, A., & Rati, Y. (2025) Optimization of microwave irradiation time for KOH-activated carbon from oil palm fronds. Acta Chimica Asiana, 8(2), 682–697. https://doi.org/10.29303/aca.v8i2.275

INTRODUCTION

Oil palm (*Elaeis guineensis*) is a major agricultural commodity, with plantations in Indonesia expanding rapidly over the past decades [1]. In 2017, the total plantation area reached 12.38 million hectares and was

projected to increase to 12.76 million hectares in 2018, distributed across 25 provinces. Riau Province has the largest coverage, spanning 2.86 million hectares as of 2020 [2].

Palm oil mills produce crude palm oil (CPO) and large amounts of biomass from shells, fronds (OPF), trunks, fibres, and empty

fruit bunches [3]. Managing this biomass is challenging due to strict environmental regulations.

Oil palm fronds are underutilized; they are often stacked or burned despite being abundant, with each tree producing 40–50 fronds annually [4]. Their physicochemical properties are summarized in Table 1.

Table 1. Physicochemical Properties of Oil Palm Fronds (OPF)

Parameter	OPF Value
Color	Yellowish brown
Density (kg/m³)	0.70-1.55
Specific gravity	< 1.00
Porosity (%)	57.9
Ash content (%)	6.7
Tensile strength (MPa)	50-400
Surface area (m²/g)	1030
Moisture content (%)	3.43
Bulk density (g/cm³)	0.56
pH	6.74

Oil palm fronds (OPF) have not yet been widely utilized as a raw material. Various conversion technologies have been developed to transform OPF and other oil palm biomass into value-added products, including biochar, bioethanol, fermentable bio-oil, sugars, biomethane, biohydrogen, nanocellulose, and compost, biocomposites. These processes employ physical, thermochemical, biological methods. The chemical composition of OPF varies with factors such as frond age, soil and climate conditions, fertilizer type, and oil palm variety; however, it generally consists of cellulose, hemicellulose, lignin, ash, and extractive compounds (Table 2) [5].

The main organic compounds in oil palm fronds, such as cellulose and lignin, provide a promising raw material for activated Durina carbonization. carbon. decompose incomplete compounds via combustion, forming a porous carbon structure that can be further activated to increase surface area and adsorption capacity [6]. Activated carbon is a carbon-rich material derived from biomass sources like coconut shells, oil palm fronds, wood, peat, or coal. It features a complex pore structure including micropores, mesopores, and macropores, as well as surface functional groups, with specific surface areas generally ranging from 500 to 3000 square meters per gram depending on the precursor and activation method [7].

Table 2. Physicochemical Characteristics of Oil Palm Fronds (OPF).

Parameter	Range Value	Description
Cellulose	40.03 -	The high
	51.50%	cellulose content
		indicates the
		potential of OPF
		as a raw material
		for cellulose-
		based materials.
Hemicellulose	17.40 –	An important
	27.08%	carbohydrate
		fraction that can
		be utilized in
		fermentation .
		processes and
		bioenergy
	4.4.40	production.
Lignin	14.49 –	A relatively lower
	22.20%	lignin content
		compared to
		hardwood, reflecting the
		characteristics of
		non-wood
		biomass.
Moisture	3.61 - 5.44%	Moisture values
Moistare	(limited)	are only available
	(mintou)	from two data
		sources: several
		studies did not
		report them (nd).
Ash	3.60 - 4.67%	Represents the
		total inorganic
		mineral content
		remaining after
		combustion.
Extractives	3.81 – 8.71%	Refers to non-
		structural
		components such
		as phenolic
		compounds and
		resins, with
		values varying
		across studies.

The production of activated carbon typically involves two stages, carbonization and activation. In carbonization, dry raw materials are heated under oxygen-free conditions below 700 degrees Celsius, causing volatile compounds to evaporate and leaving a carbon-rich solid known as charcoal or biochar. Activation expands the pore structure, creating a microscopic network within the carbon. Activation can be physical or chemical, each with distinct mechanisms [8].

Chemical activation, particularly using Potassium Hydroxide, is effective for materials with high cellulose content. The process involves mixing the precursor with Potassium Hydroxide and heating at high temperatures to

develop a well-distributed pore structure. Potassium Hydroxide is favoured over other activators, such as Potassium Carbonate, zinc chloride, or phosphoric acid, because it produces fine pores, has a lower environmental impact, is less corrosive, and is cost-effective. Potassium Hydroxide-activated carbon exhibits high adsorption efficiency for organic pollutants, heavy metals, dyes, and pesticides, though its yield of 10 to 40 per cent is lower compared to some other activators [9].

The surface area is the most important characteristic of activated carbon. Various synthesis methods have been explored to increase this surface area. Zikri et al. (2022) [6] found that charcoal from oil palm fronds had a moisture content of 2.39% and an ash content of 9.96%. The height (Lc) and width (La) of microcrystalline stacks, as well as the Lc/La ratio, indicate the surface area. The carbonization at 600 °C produced the highest Lc/La ratio of 0.407, where a higher ratio corresponds to a smaller crystal size and a larger adsorption surface area [10].

Natasyah, 2020 [11] demonstrated that chemical activation with a charcoal-to-KOH ratio of 1:3 increased the Lc/La ratio from 0.407 to 1.956, significantly enhancing the surface area. Zikri (2024) [12] further synthesized potassium hydroxide-activated carbon and combined it with magnetite for the Fenton degradation of Methylene Blue. The MACOPF 1 catalyst degraded 95.88 % of Methylene Blue, although the Lc/La ratio decreased slightly due to partial pore occupation by magnetite. BET analysis confirmed this trend, showing that the surface area increased from 163.98 m²/g for charcoal (COPF) to 605.84 m²/g after KOH activation (ACOPF).

Physical activation forms through heat treatment, typically at 800 to 900 °C, and can also be performed using microwave-based heating [13]. Microwave radiation is type of non-ionising а electromagnetic radiation with a frequency range of 300 MHz to 300 GHz and a wavelength of 1 meter to 1 millimetre. Microwave heating in the pyrolysis process offers several advantages over conventional methods, including higher energy efficiency, rapid heating, selective and internal heating, enhanced chemical reactivity, reduced waste volume, ease of process control, flexibility, portability, cost-effectiveness, and higher safety and automation levels [13].

This technology has been successfully applied to the preparation and regeneration of

activated carbon from agricultural biomass. Before treatment, the biomass is washed with deionized water to remove impurities, dried at 65–105 °C, and ground to reduce particle size, which promotes uniform heating. Activated carbon efficiently absorbs microwave energy through dipole rotation and ionic conduction, allowing rapid treatment within minutes. Microwave activation of mesoporous carbon, particularly using potassium hydroxide at 973 K, can generate a large number of micropores while preserving the existing mesoporous structure, enhancing adsorption capacity [14].

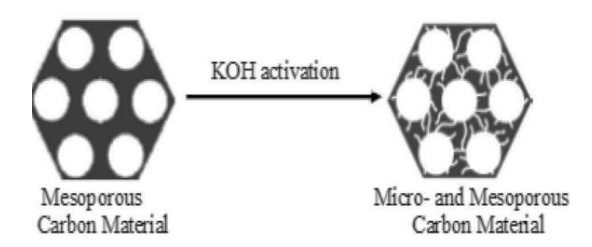


Figure 1. Formation process of micropores in mesoporous carbon activated with KOH at 973 K [13]

The production of activated carbon from agricultural biomass using microwave technology is strongly influenced by factors such as microwave power, irradiation time, and the type and concentration of chemical activating agents. These factors directly affect carbon yield and adsorption capacity. Irradiation time is particularly critical, as prolonged exposure accelerates heating, enhances reaction kinetics, and promotes the formation of a complex pore structure. Optimum irradiation achieves a balance between absorbed and reflected energy, resulting in maximum adsorption capacity. Microwave heating offers several advantages, including lower energy consumption, shorter processing times, and the reduction of elements such as oxygen and potassium through evaporation during activation [15].

Microwave-assisted activation gained attention as an efficient alternative to conventional high-temperature carbonization and activation methods due to its shorter processing time, reduced energy consumption, and ability to produce activated carbon (AC) with well-developed porosity. Duran et al, 2024 demonstrated that а single-step microwave-assisted activation process using potassium hydroxide (KOH) can convert lignocellulosic precursors into ACs with high specific surface areas (up to 1340 m²/g) and strong CO₂ adsorption capacity. Among the tested materials, pine wood-based AC

exhibited the best performance, characterized by high carbon content (79%), amorphous structure, large ultra-micropores, and excellent CO_2/N_2 selectivity (12.5).

Several other studies have explored microwave-assisted activation using local biomass feedstocks. Komariyah, 2021 [17] showed that a 1:1 charcoal-to-KOH ratio reduced colour and turbidity in palm oil effluent by 94.54%, although the low Lc/La ratio indicated incomplete graphitic (0.089)ordering. Wahyuni (2021) [18] reported the highest carbon content (66.79%) at the same ratio, suggesting potential for enhanced pore formation. In contrast, Taufik et al. (2021) [19] found that iodine adsorption increased with irradiation time and power, but then declined due to excessive exposure. The resulting ACs met SNI 06-3730-1995 standards. demonstrating good Pb2+ adsorption capacity mg/g) consistent with Langmuir behaviour. Similarly, Zalmi et al. (2021 [20] achieved optimal Rhodamine B adsorption (7.25 mg/g) using sugarcane bagasse as a precursor. Extended microwave exposure accelerates activation and pore development. but excessive energy input leads to localized overheating, pore collapse, and reduced surface area [21].

valuable Despite these findings, significant gaps remain in understanding how microwave power intensity and irradiation duration quantitatively influence the structural evolution, porosity, and adsorption behaviour of the resulting AC. Most previous studies used relatively low power levels (around 100 W), resulting in limited activation efficiency, carbon content, and lower incomplete graphitization. Moreover, the interrelationship between activation parameters and key material properties. such as surface morphology, lattice ordering, and functional composition, has not systematically investigated. These limitations hinder the optimization and scalability of microwave-assisted activation for sustainable AC production from diverse biomass sources.

Therefore, this study addresses these research gaps by employing higher microwave power (200 W) and varying irradiation durations of 5, 10, and 15 minutes following chemical activation. The systematic evaluation of yield, moisture, and ash content, iodine adsorption capacity, crystal structure (XRD), surface morphology and composition (SEM-EDX), and functional groups (FTIR) aims to provide a more comprehensive understanding of the relationship between the input of

activation energy, pore formation, and adsorption performance. The results are expected to establish a rational basis for designing energy-efficient, high-performance activated carbon from biomass precursors while contributing to the broader development of sustainable materials for environmental remediation.

MATERIALS AND METHODS

Materials

The primary raw material used in this study was oil palm fronds collected from the area of Jl. Suka Karya, Tuah Karya Village, Tampan District, Pekanbaru Regency, Riau Province. The chemicals employed included potassium hydroxide (KOH, Merck) for the chemical activation process, as well as several reagents for the analysis of Fe(III) content, namely hydrochloric acid (HCI) and sulfuric acid (H₂SO₄) (both from Smart Lab), potassium iodide (KI), potassium iodate (KIO₃), iodine (I₂), sodium thiosulfate (Na₂S₂O₃), and starch as an indicator, all supplied by Merck. In addition, a pH 7 buffer solution, Whatman No. distilled water, filter paper, demineralized water (DM water) were used as solvents and washing agents during the preparation and analysis processes.

Equipment

The equipment used in this study included a Nabertherm furnace for the carbonization of materials and a Panasonic convection microwave oven for the post-carbonization activation process. Initial drying of the samples was performed using a Memmert UNB 400 oven (53 L), while material weighing was carried out with an ABJ 320-4NM analytical balance to ensure high accuracy.

Solution stirring was conducted using a REXIM RSH-1DR hotplate stirrer and a magnetic stirrer. The pH of the solutions was measured using a digital pH meter, and the samples were stored in a desiccator containing silica gel to maintain dryness. Sample preparation involved a mortar and pestle, followed by sieving through 100–200 mesh sieves to obtain uniform particle size distribution.

Standard glassware, including burettes, pipettes, beakers, and Erlenmeyer flasks, was used throughout the solution preparation and analysis stages. Material characterization was performed using X-Ray Diffraction (XRD) X'Pert PRO PANalytical for

crystal structure analysis, and Scanning Electron Microscopy (SEM) JEOL JSM-6510LA equipped with Energy Dispersive X-ray Spectroscopy (EDX) for observing surface morphology and analyzing elemental composition.

Procedure

a. Collection and Preliminary Processing of Charcoal from Oil Palm Fronds (OPF)

Oil palm fronds (OPF) were collected from Jl. Suka Karya, Desa Tuah Karya, Kecamatan Tampan, Kabupaten Pekanbaru, Riau Province. The OPF was cut into approximately ±2 cm pieces, washed with deionized water to remove impurities, sundried, and then oven-dried at 105 °C for 24 h to minimize moisture content.

Following the method developed by [6], the dried OPF was carbonized in a furnace at 600 °C for 60 minutes to obtain carbonized oil palm frond charcoal (COPF). The resulting material was ground and sieved using 100–200 mesh sieves. The fraction retained on the 200-mesh sieve was selected, stored in airtight plastic bags, and kept in a desiccator until further use.

b. Activation of Oil Palm Frond Activated Carbon

Chemical activation of COPF was conducted using a potassium hydroxide (KOH) solution with a mass ratio of 1:1 (g/g) between COPF and KOH (1% m/v) dissolved in 100 mL of deionized water, following [17]. The mixture was heated on a hot plate stirrer at 300 rpm and 100°C for 6 hours to ensure proper impregnation, then filtered using Whatman No. 42 paper.

Physical activation was carried out using a microwave convection oven at 200 W for 5, 10, and 15 min, designated as A5D200, A10D200, and A15D200, respectively. After activation, the samples were washed with 1 M HCl and deionized water, monitoring the pH until the filtrate reached neutrality (pH 7). The neutralized samples were oven-dried at 105°C for 24 h and stored in a desiccator to prevent moisture absorption.

c. Characterization of Activated Carbon

1. Yield

Yield determination was performed to evaluate the conversion efficiency from raw OPF to activated carbon. The percentage yield was calculated using:

$$= \frac{Weight\ of\ final\ product}{/Weight\ of\ initial\ material} x100\%$$

2. Moisture Content (SNI 06-3730-1995)

Approximately 0.1 g of each sample was placed in a pre-weighed crucible and heated at 105°C for 1 h. After cooling in a desiccator, the crucible was reweighed until a constant mass was achieved. The moisture content was determined using:

$$Moisture\ content(\%) = \frac{a-b}{a}x100\%$$

where *a* is the initial weight and *b* is the dried weight of the sample.

3. Ash Content (SNI 06-3730-1995)

About 0.5 g of each sample was placed in a crucible and heated in a furnace at 900°C for 1 hour. After cooling in a desiccator, the sample was weighed until a constant mass was obtained. Ash content was calculated as:

$$Ash\ content(\%) = \frac{Weight\ of\ ash}{Weight\ of\ material} x 100\%$$

4. Iodine Adsorption Test (I_2) (SNI 06-3730-1995)

A total of 0.5 g of activated carbon was mixed with 50 mL of 0.1 N iodine solution and stirred for 15 minutes, followed by standing for 1 hour and then centrifugation for 15 minutes. A 5 mL aliquot of the supernatant was titrated with 0.1 N sodium thiosulfate using 1% starch indicator. The iodine adsorption capacity (I) was calculated using:

$$I = \frac{(V1N1 - V2N2) \times Mr \times fk)}{Wo}$$

Description:

I = Amount of iodine adsorbed (mg/g)

 V_1 = Initial volume of iodine solution (mL)

 V_2 = Volume of sodium thiosulfate solution used (mL)

 N_1 = Normality of iodine solution

 N_2 = Normality of sodium thiosulfate solution

Mr = Molar mass of iodine (126.92 g/mol)

fk = Conversion factor (10)

 $W_0 = Sample weight (g)$

5. Determination of Lattice Parameters and Degree of Crystallinity Using X-Ray Diffraction (XRD)

X-ray diffraction (XRD) analysis was performed on A5D200, A10D200, and A15D200 samples to determine lattice parameters and crystallinity. The samples were prepared as pellets and scanned over 0°–90° (2θ). Diffraction data were analyzed using Origin software to calculate the graphitic stacking height (Lc), lateral crystallite size (La), and degree of crystallinity. All XRD analyses were conducted at the Materials Laboratory, Department of Physics, Universitas Negeri Padang.

6. Determination of Surface Morphology and Elemental Composition Using Scanning Electron Microscopy–Energy Dispersive X-Ray Spectroscopy (SEM-EDX)

Surface morphology and elemental composition of the A5D200, A10D200, and A15D200 samples were analyzed using Scanning Electron Microscopy (SEM) and Energy Dispersive X-Ray Spectroscopy (EDX) at magnifications of 2500× and 7500×. Analyses were conducted at the Mechanical Engineering Laboratory, Institut Teknologi Sepuluh Nopember (ITS), Surabaya.

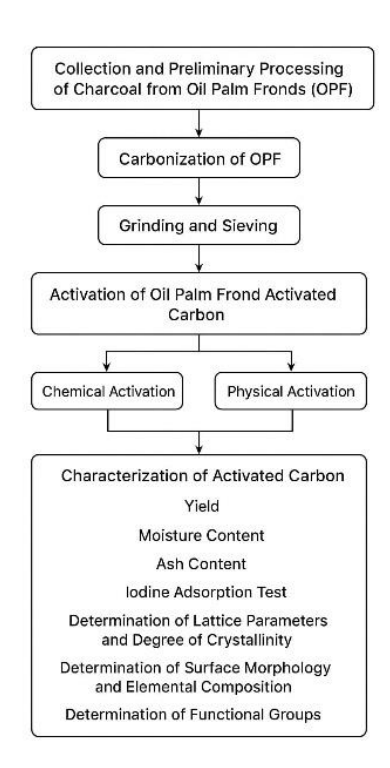


Figure 2. Flowchart of the experimental procedure in this study.

7. Determination of Functional Groups using Fourier Transform Infrared (FTIR)

Fourier Transform Infrared Spectroscopy (FTIR) was used to identify functional groups in the activated carbon samples. Finely ground samples were mixed with KBr, pressed into pellets, and analyzed by scanning to determine the chemical functionalities present.

8. Statistical Validation

The data obtained from three replications were averaged, and the mean values were used for further analysis to ensure data consistency and accuracy.

9. Experimental Flowchart

The flowchart for this study is presented in Figure 2.

RESULTS AND DISCUSSION

T-1-1-

1. Characterization of COPF and Activated Carbon A5D200, A10D200, and A15D200

The characteristics of carbonized oil palm fronds (COPF) and their activated variants (A5D200, A10D200, and A15D200) were evaluated through moisture content, ash content, and iodine adsorption capacity tests according to SNI 06 3730 1995. Yield and surface area were also calculated to provide a broader understanding of production efficiency and adsorption potential. The results of these analyses are presented in Table 3.

01-----

Table Physico	-	haracteri I Properti		of Yield	d and
Sampl e Code	Yield (%)	Moist ure Conte nt (%)	Ash Conte nt (%)	Iodine Adsorpt ion Capacit y (mg/g)	Surfa ce Area (m²/g)
COPF	21.19	3.26	12.47	544.22	541.3 9
A5D20 0	91.32	0.29	6.07	776.59	772.4 4
A10D2 00	91.04	0.99	6.92	828.69	824.2 6
A15D2 00	84.77	0.80	6.46	692.03	688.3 3
SNI Standa rd	not specifi ed	≤ 15	≤ 10	≥ 750	not specifi ed

Chemical activation using KOH followed by microwave irradiation significantly improved the physicochemical properties of the carbon material compared to simple carbonization (COPF) [22]. These improvements directly influenced adsorption

of Mintal and

performance because yield, moisture, and ash contents collectively determine structural integrity and the availability of active sites for adsorbate interaction.

Yield reflects the efficiency converting biomass into activated carbon and indicates process effectiveness as well as its implications for cost, material utilization, and sustainability [23]. The COPF sample. produced solely by carbonization, showed a low yield of 21.19 percent due to extensive decomposition of cellulose, hemicellulose, and lignin, which limited stable carbon formation [24]. Without KOH activation, the development of aromatic and porous carbon frameworks was hindered, confirming the low thermal efficiency of conventional carbonization [25].

KOH-activated and microwave-treated samples (A5D200 and A10D200) achieved significantly higher yields of 91.32% and 91.04%, respectively. The reaction between KOH and carbon during heating promoted the formation of stable porous structures, while microwave energy ensured uniform heating and minimized degradation [26]. However, prolonged irradiation reduced the yield of A15D200 to 84.77 % due to overactivation, which caused pore collapse, gas release, and the formation of soluble species such as K_2CO_3 and K_2O [27].

Although the yield of A15D200 remained higher than that of COPF, the decrease corresponded with reduced iodine adsorption and surface area, showing that high yield does not always indicate superior adsorption when pore structure is damaged. Yields close to 90 %, as in A5D200 and A10D200, reflect efficient biomass utilization production and cost-effective must be Nonetheless. yield evaluated adsorption alongside surface area and capacity, as optimal activated carbon should combine high yield, well-developed porosity, and structural stability, as demonstrated by A10D200.

Moisture content is a key parameter influencing the adsorption efficiency and stability of activated carbon. In this study, moisture content decreased significantly after KOH activation and microwave irradiation compared to the carbonized sample (COPF). COPF exhibited 3.26 %, while A5D200, A10D200, and A15D200 dropped to 0.29, 0.99, and 0.80 %, respectively, indicating effective removal of trapped water and enhanced pore formation.

Lower moisture generally improves adsorption by preventing water from blocking

active sites. However, the highest iodine adsorption in A10D200 rather than A5D200 suggests that pore connectivity and structural development also determine adsorption performance [29,30]. Excessively moisture, as in A15D200, may indicate partial thermal degradation associated with reduced yield and adsorption capacity. Therefore, moisture content must be optimized alongside other process parameters to maintain structural integrity and maximize adsorption efficiency [31].

Ash content reflects the presence of inorganic materials in activated carbon and strongly affects adsorption performance. High ash may indicate incomplete carbonization, mineral contamination, or residual activating agents. The non-activated COPF sample had an ash content of 12.47 %, exceeding the SNI limit (≤10 %), due to inherent minerals in palm fronds and insufficient carbonization under air at 600 °C for 60 minutes [32]. Carbonization in the absence of an inert gas allows oxidation of metallic elements, further increasing ash [33].

KOH activation combined with microwave irradiation reduced ash in A5D200, A10D200, and A15D200 to 6.07, 6.92, and 6.46 %, respectively. Short irradiation in A5D200 efficiently removed minerals without damaging the structure, while longer irradiation in A10D200 enhanced demineralization. Excessive irradiation in A15D200 caused partial framework degradation and volatilization of some inorganic species [34].

Ash content directly affects adsorption because excessive ash blocks pores. COPF, with the highest ash, had the lowest iodine adsorption (544.22 mg/g), whereas A10D200, with optimal ash and well-developed pores, achieved the highest adsorption (828.69 mg/g). A15D200, despite similar ash, showed reduced adsorption (692.03 mg/g) due to pore damage from overactivation [35]. Thus, ash content is a key indicator of demineralization efficiency, thermal stability, and the integrity of pore structure. It must be balanced to remove inorganic compounds while preserving the carbon framework essential for adsorption [36].

lodine adsorption capacity and surface area are key indicators of activated carbon performance, strongly influenced by pore structure, activation type, and surface chemistry. The non-activated COPF exhibited the lowest adsorption capacity (544.22 mg/g) and surface area (541.39 m²/g) due to the absence of chemical or thermal activation, as

well as its high moisture and ash content, which blocked pores [37].

KOH activation combined with microwave irradiation improved both parameters. A5D200, irradiated for five minutes, achieved 776.59 mg/g and 772.44 benefitina from initial micropore m²/a. formation and reduced moisture (0.29%) and ash (6.07%).Optimal conditions were achieved in A10D200 with ten-minute irradiation, resulting in 828.69 mg/g and 824.26 m²/g, as pores were fully developed without structural damage and with low moisture and ash content [38].

Overactivation in A15D200 (15 minutes) caused pore collapse and partial degradation, reducing adsorption capacity to 692.03 mg/g and surface area to 688.33 m²/g, despite low moisture and ash. It demonstrates that large surface area alone does not guarantee high adsorption; uniform, stable micropores are essential. Consequently, A10D200 exhibited the best balance of chemical reactivity, structural integrity, and pore accessibility [39].

Ates et al. (2023) [40] conducted a study using raw tea waste (RTW) as a biochar precursor, which was pyrolyzed at 300 and 500 °C following chemical activation with H_3PO_4 (85%) or KOH (3 M), as well as physical treatments involving ultrasound and microwave irradiation. The resulting biochar exhibited ash contents ranging from 2% to 7% after KOH activation. This range is comparable to our activated carbon samples A5D200, A10D200, and A15D200, which also showed ash contents within a similar interval. These findings indicate that KOH activation effectively reduces ash content and enhances the purity of activated carbon derived from biomass. Similar to Aloud et al. (2023 [41]), who reported a moisture content reduction from 5.75 to 3.38% in microwave-activated carbon, the moisture content in this study also decreased significantly from 3.26 to 0.29% after KOH activation and microwave irradiation of raw biomass.

Ahmad et al, 2021 [42] found that the optimum conditions for microwave-assisted activation were 700 W of power, a K_2CO_3/C ratio of 1.5:1, and a radiation time of 30 minutes, yielding activated carbon with an iodine number of 1834 mg/g, methylene blue adsorption of 517.5 mg/g, and a yield of 16.65 %. In comparison, the activated carbon produced in this study showed iodine numbers ranging from 544.22 to 828.69 mg/g, indicating

moderate adsorption performance relative to the optimal conditions reported by Li et al.

This study demonstrates that carbon derived from oil palm fronds without activation (COPF) exhibits suboptimal performance. This is reflected in the low yield, which did not reach 50 %, as well as in the high levels of moisture and ash content. In contrast, the samples that underwent chemical activation and microwave heating (A5D200, A10D200, and A15D200) showed better quality and complied with the requirements of SNI No. 06-3730-1995 for moisture and ash parameters. Nevertheless, the iodine adsorption capacity of the A15D200 sample still did not meet the threshold of the standard.

2. Identification of Functional Groups

Activated carbon from oil palm fronds was produced by heating at 600°C for 1 hour, followed by chemical activation with KOH at a 1:1 mass ratio in 100 mL of demineralized water. The samples were then irradiated in a microwave for 5, 10, and 15 minutes at 200 W. Functional groups were identified using FTIR for A5D200, A10D200, A15D200, and non-activated carbon (COPF). All spectra are presented together in Figure 3.

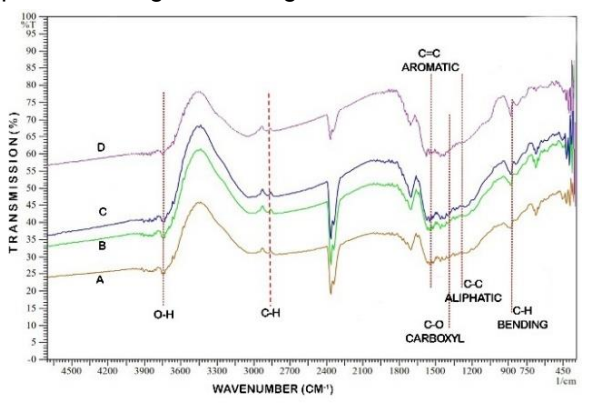


Figure 3. FTIR spectra (a) A5D200 (b) A10D200 (c) A15D200 (d) COPF

FTIR analysis revealed significant changes in functional groups on activated carbon surfaces after KOH activation and microwave irradiation. The non-activated sample (COPF) showed low O–H stretching intensity (3200–3700 cm⁻¹), indicating limited hydroxyl groups and low hydrophilicity, consistent with its high moisture (3.26%) and ash content (12.47%), low yield (21.19%), and poor iodine adsorption capacity (544.22 mg/g) and surface area (541.39 m²/g) [6,43].

A5D200 showed increased O-H intensity, the appearance of C=O stretching

(~1700 cm⁻¹), and sharper aromatic C=C bands, reflecting the introduction of polar groups and reinforced aromatic structure. These changes, combined with low moisture content (0.29%) and ash content (6.07%), and high yield (91.32%), contributed to enhanced pore formation and a high iodine adsorption

capacity of 776.59 mg/g and a surface area of 772.44 m²/g [6].

The identification of functional groups in the activated carbon samples COPF, A5D200, A10D200, and A15D200 is summarised in Table 4.

|--|

Functional	Group	Wavenumber Range (cm⁻¹)	COPF	A5D200	A10D200	A15D200	Reference
O–H stretchi	ing	3200 to 3700	3650.50	3713.13	3650.44	3713.13	(Adame-Pereira et al. 2021)
Aliphatic stretching	C–H	2850 to 3000	2827.64	2865.38	2866.34	2871.17	(Adame-Pereira et al. 2021)
Aromatic stretching	C=C	1400 to 1500	1420.33	1437.03	1439.50	1496.83	(Zikri et al. 2022)
Carbonyl stretching	C=O	1600 to 1820	1650.32	1701.29	1800.63	1701.29	(Adame-Pereira et al. 2021)
Aliphatic C-	C bond	1289 to 1395	1288.50	1287.54	1288.50	1288.50	(Zikri et al. 2022)
C–O s (carboxylic a	stretching acid)	1200 to 1400	1250.25	1308.76	1308.76	1308.76	(Opoku et al. 2021)
C-H bending	g	Around 827	800.46	874.76	877.65	875.72	(Opoku et al. 2021)

Extending microwave irradiation to 10 minutes in A10D200 produced the most intense and sharp FTIR bands, indicating the highest concentration of surface-active groups, optimal pore development, and a stable carbon framework. Consequently, moisture (0.99%) and ash (6.92%) remained low, yield was maintained (91.04%), and iodine adsorption reached its maximum (828.69 mg/g) with the largest surface area (824.26 m²/g) [41,44].

Prolonged irradiation for 15 minutes in A15D200 caused decreased O–H and C–H intensities and slight shifts in C=C and C=O peaks, indicating partial decomposition of functional groups and potential pore collapse. It corresponded with reduced yield (84.77%), iodine adsorption (692.03 mg/g), and surface area (688.33 m²/g), despite acceptable moisture (0.80%) and ash (6.46%) levels [41].

Overall, FTIR spectra correlate closely with adsorption performance, as also reported by [43,45,46]. The abundance and stability of polar functional groups (O–H, C=O) and aromatic structures (C=C) determine the number and quality of active adsorption sites, directly influencing the adsorption capacity and surface reactivity of the activated carbon. Moisture, ash, and yield reflect surface cleanliness and framework stability, and all these factors synergistically govern iodine adsorption capacity and surface area. The A10D200 sample achieved an optimal balance, where the development of functional groups, pore formation, and structural integrity

collectively resulted in the highest adsorption performance [47].

3. Determination of lattice parameters and degree of crystallinity using X Ray Diffraction (XRD)

The lattice structure and crystallinity of activated carbon samples A5D200, A10D200, and A15D200 were analyzed using X Ray Diffraction (XRD). The resulting diffraction patterns for all samples are shown in Figure 4.

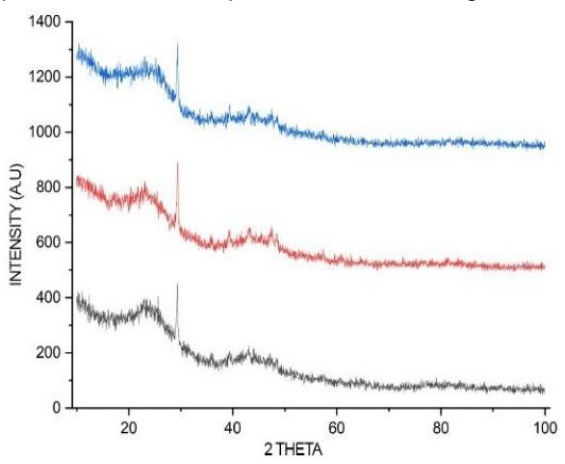


Figure 4. XRD diffractogram of (a) A5D200, (b) A10D200, and (c) A15D200

X-ray Diffraction (XRD) characterization was performed to investigate the lattice structure of activated carbon, including interplanar spacing (d), the positions of the (002) and (100) peaks, lattice parameters (Lc and La), and the Lc/La ratio.

All data were analyzed using Microcal Origin software and are summarized in Table 5

The degree of crystallinity was determined from the ratio of the crystalline

area to the total diffraction area using Origin Pro software. The crystallinity and amorphous characteristics of each sample are presented in Table 6.

Table 5. Lattice structure parameters of activated carbon based on XRD analysis

Sample	2θ (002)	2θ (100)	d (002) (nm)	d (100) (nm)	Lc (nm)	La (nm)	Lc/La
A5D200	23.001	45.673	3.863	1.984	7.655	2.678	2.858
A10D200	23.142	45.890	3.849	2.045	8.022	2.698	2.916
A15D200	23.000	44.700	3.863	2.025	6.345	2.840	2.234

Table 6. Percentage of crystallinity and amorphous phase of activated carbon based on XRD results.

Sample	Crystalline Area	Total Area	% Crystallinit y	% Amorphous
A5D200	872.527	9734.038	8.96%	91.04%
A10D200	1075.569	8923.425	12.05%	87.95%
A15D200	2561.374	9090.205	28.18%	71.82%

From the data above, it can be seen that the longer the microwave heating time, the greater the increase in crystallinity of activated carbon, while the amorphous structure decreases. The XRD diffractogram in Figure 2 shows a main peak at around $2\theta = 23^{\circ}$, identified as the (002) plane, and a minor peak at around $2\theta = 45-46^{\circ}$, corresponding to the (100) plane [45], characteristic of graphitic structures in activated carbon. The presence of these peaks indicates a mixture of amorphous and crystalline phases [48]. These results are consistent with those of Ates et al. (2023) [49], who also reported that microwaveassisted activation promotes the development of graphitic domains, resulting in enhanced crystallinity and improved carbon structure ordering.

The increasing intensity sharpness of the peaks from A5D200 to A15D200 demonstrate that longer microwave activation (from 5 to 15 minutes) increases crystallinity, as supported by Table 6, where crystallinity rises from 8.96% (A5D200) to 12.05% (A10D200) and reaches 28.18% (A15D200). This increase results from the rearrangement of graphitic structures, allowing carbon atoms to form more ordered layers. However, higher crystallinity often reduces surface area and microporosity, which are critical for adsorption, explaining the inverse relationship with iodine adsorption performance [50].

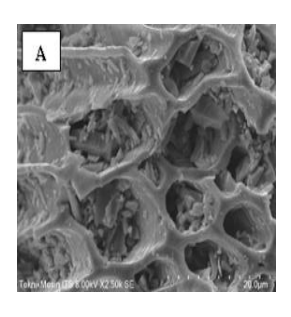
The A5D200 sample exhibited a predominantly amorphous structure (91.04%) with relatively high Lc (7.655 nm) and La (2.678 nm), resulting in an Lc/La ratio of 2.858. This high amorphous fraction promotes the

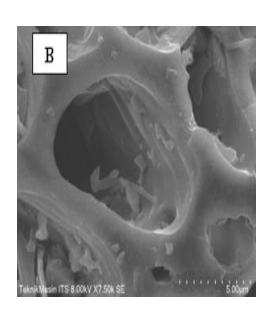
development of irregular micropores, which are essential for adsorbing small molecules, such as iodine (Farma et al., 2022). The combination of low moisture (0.29%), low ash content (6.07%), and high yield (91.32%) further supports the accessibility of the active site. Consequently, the iodine adsorption capacity (776.59 mg/g) and surface area (772.44 m²/g) are high, demonstrating that a lower crystallinity, accompanied by abundant micropores and functional groups (confirmed by FTIR), strongly enhances adsorption performance [51].

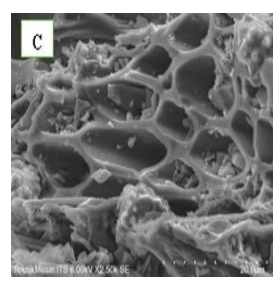
A10D200 represents an optimal balance between crystalline and amorphous structures. Crystallinity increased moderately to 12.05%, while the amorphous fraction remained dominant at 87.95%, with Lc = 8.022 nm and Lc/La = 2.916. The moderate increase in the Lc/La ratio supports an expanded surface area and stable pore channels, which, together with the abundance of O-H and C=O groups observed in FTIR, enhance interactions with iodine molecules. These structural superior features enable adsorption performance, reflected in the highest iodine adsorption capacity (828.69 mg/g) and largest surface area (824.26 m²/g). It demonstrates that moderate crystallinity stabilizes the carbon framework while maintaining active micropores critical for adsorption [10,52].

In contrast, A15D200 showed high crystallinity (28.18%) and reduced amorphous content (71.82%). Lc decreased to 6.345 nm, and the Lc/La ratio dropped to 2.234, suggesting partial collapse of vertical crystalline layers due to excessive heating. Although La increased slightly (2.840 nm),

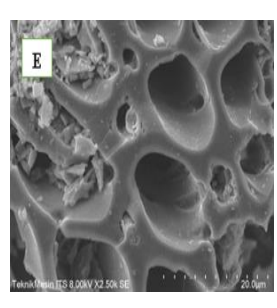
surface area and microporosity decreased, resulting in lower iodine adsorption capacity (692.03 mg/g) and surface area (688.33 m²/g). The decrease in polar functional group intensity (FTIR) indicates a loss of active sites, while low moisture content (0.80%) and ash content (6.46%) cannot compensate for structural degradation. The reduction in yield (84.77%) further reflects carbon loss and pore collapse. These observations confirm that excessive crystallinity diminishes adsorption performance by reducing the number of accessible micropores and active sites [53].











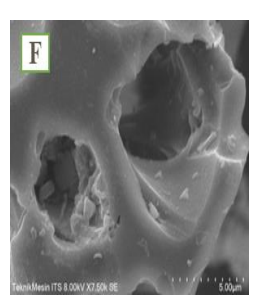


Figure 5. Surface morphology of activated carbon: (a) A5D200 at 2500× magnification, (b) A5D200 at 7500× magnification, (c) A10D200 at 2500×, (d) A10D200 at 7500×, (e) A15D200 at 2500×, and (f) A15D200 at 7500×.

Overall, XRD parameters such as crystallinity, Lc, La, and Lc/La ratio correlate strongly with adsorption capacity. Low-to-moderate crystallinity, combined with high amorphous content, favours the development of micropores, increased active site exposure, and a high surface area, resulting in improved

iodine adsorption. Conversely, excessive crystallinity stabilizes the structure but reduces micropore volume and active sites, limiting adsorption. Therefore, balancing crystalline and amorphous structures, as seen in A10D200, is crucial for achieving optimal activated carbon performance [6]

4. Surface Morphology and Elemental Composition Analysis

The surface morphology and elemental composition of activated carbon samples (A5D200, A10D200, A15D200) prepared via carbonization, KOH activation, and microwave treatment are shown in Figure 5, highlighting the effects of activation and heating duration on pore structure and adsorption-related surface properties.

The chemical composition of activated carbon derived from oil palm fronds was analysed using Energy Dispersive X-Ray Spectroscopy (EDX), with spectra plotted on the x-axis as energy (keV) and on the y-axis as relative intensity (wt%). Results for A5D200, A10D200, and A15D200 are summarized in Table 7. Additionally, average pore sizes were determined from SEM images using ImageJ software, with the data presented in Table 8.

Table 7. Chemical element composition of activated carbon based on EDX analysis

Element	A5D200	A10D200	A15D200
	(wt%)	(wt%)	(wt%)
С	43.6	56.0	69.0
N	12.7	3.0	4.0
0	37.1	28.0	17.0
CI	0.3	3.0	3.0
Ca	6.4	10.0	8.0

Note: wt% = weight percentage of elements based on EDX measurement

Table 8. Average pore size of activated carbon based on SEM images analyzed using ImageJ software

No	Sample	Average Pore Size (µm)
1	A5D200	7.6276
2	A10D200	6.6610
3	A15D200	8.2866

Sample A5D200 (Figures 3a and 3b) exhibits a surface with well-distributed pores of various sizes and relatively thin but irregular pore walls, similar to the findings of [6,49]. Sample A5D200 (Figures 3a–3b) shows well-distributed pores with irregular, thin walls and an average pore size of 7.63 μm , facilitating iodine diffusion. The high oxygen content (37.1 wt%) and active polar groups (–OH, C=O),

confirmed by FTIR, act as adsorption sites. Combined with low moisture (0.29%), low ash (6.07%), high yield (91.32%), and an amorphous structure (91.04%), these features result in high iodine adsorption (776.59 mg/g) and large surface area (772.44 m²/g) [54].

Sample A10D200 (Figures 3c-3d) exhibits more uniform pores (6.66 µm) with denser walls and a more stable carbon framework from 10-minute microwave activation. Carbon content increased to 56 wt% while oxygen and nitrogen decreased, though remaining polar groups are active. Moderate crystallinity (12.05%) maintains pore stability, supporting the highest iodine adsorption (828.69 mg/g) and surface area (824.26 m²/g), with well-controlled moisture (0.99%), ash (6.92%), and yield (91.04%) [54,55]. A10D200 represents the optimal adsorbent due to synergy between morphology, functional groups, and microstructure.

Sample A15D200 (Figures 3e–3f) shows larger, irregular pores (8.29 µm) with thickened walls partially blocked by residual particles. Carbon content rose to 69 wt% while oxygen dropped to 17 wt%, indicating loss of polar groups. Higher crystallinity (28.18%) and reduced amorphous fraction caused partial pore collapse, leading to lower surface area (688.33 m²/g) and iodine adsorption (692.03 mg/g), with a reduced yield (84.77%) [56].

Overall, SEM and pore size analysis provide both visual and quantitative evidence of the effectiveness of the activation process in forming active pore structures. However, adsorption performance depends not only on pore size but also on surface chemical composition, structural stability, and the optimal amorphous-to-crystalline ratio. A10D200 exhibits the best balance among these factors, whereas A5D200 excels in polar group activity and pore distribution, and A15D200 shows limitations due to structural degradation caused by excessive thermal treatment.

Activated carbon A10D200, derived from oil palm fronds via KOH activation and 10-minute microwave irradiation, exhibited the best adsorption performance among the samples. SEM images revealed uniform pores (6.66 µm) with stable walls, supporting efficient diffusion of adsorbates. EDX analysis showed balanced carbon and oxygen content, indicating the presence of polar functional groups. FTIR spectra confirmed the presence of abundant and stable O-H and C=O groups, which serve as active sites for adsorption.

XRD results indicated moderate crystallinity (12.05%) with a high amorphous fraction (87.95%), ensuring structural stability while maintaining accessible micropores.

The synergy of well-developed pores, active functional groups, and an optimal amorphous-to-crystalline ratio led to the highest iodine adsorption capacity (828.69 mg/g) and surface area (824.26 m²/g). These results demonstrate that adsorption efficiency depends not only on surface area but also on pore structure, surface chemistry, and microstructural stability, making A10D200 the most effective adsorbent in this study.

CONCLUSION

In conclusion, the longer the microwave irradiation time, the lower the yield and moisture content of the A5D200, A10D200, and A15D200 samples tended to be. Nevertheless, all samples met the quality standards of activated carbon according to SNI No. 06-3730-1995, both in terms of moisture and ash content. The iodine adsorption test showed a direct correlation with the surface area of activated carbon. The adsorption capacity increased with irradiation time but began to decrease at 15 minutes of irradiation. The sample with the highest iodine adsorption was A10D200, and both A10D200 and A15D200 fulfilled the SNI standard for iodine adsorption capacity (≥750 mg/g). Second, characterisation using Diffraction (XRD) revealed two main peaks in the range of 22.843°-23.001° and 43.740°-45.673°, corresponding to the (002) and (100) crystal planes, respectively, confirming the amorphous nature of the activated carbon. A longer microwave heating duration resulted in an increased Lc/La ratio and degree of crystallinity, indicating an expansion of the carbon surface area. From SEM analysis, the surface morphology of A5D200 and A15D200 still showed the presence of impurities and pore damage, whereas A10D200 exhibited cleaner pores with smaller sizes and more uniform distribution. The carbon content also increased with longer irradiation times. Based on FTIR analysis, shifts in wavenumber and absorption band intensity were observed, indicating the presence of various functional groups, such as O-H (alcohol, phenol, and carboxylic acid), aliphatic C-H, C-H bending, aromatic C=C, carbonyl (C=O), nitrile (C=N), aliphatic C-C, and C-O from carboxylate compounds. Overall, these results indicate that microwave activation at 200 W for 10 minutes optimally enhanced pore structure, functional group availability, and adsorption efficiency, making A10D200 the most effective activated carbon from oil palm fronds.

Acknowledgements

The author would like to express sincere gratitude to Dr Muhdarina, M.Si., for the guidance, advice, and support provided throughout this research. Her presence has been of great help in ensuring the smooth implementation of the research, data collection, and preparation of the research findings. May all the assistance and dedication she has given become a lasting virtue and bring broad benefits.

REFERENCES

- [1] Syafrani, S., Purnama, I., Mutamima, A., & Dewi, W. N. (2022). Study on the commitment of oil palm companies to achieve sustainable agriculture in Riau Province from the perspective of pesticide use. *IOP Conference Series: Earth and Environmental Science, 1041*(1), 012038.
- [2] Ismiasih, I., & Afroda, H. (2023). Faktor penentu produksi kelapa sawit rakyat di Provinsi Riau. *Jurnal Penelitian Pertanian Terapan*, 23(3), 211–218.
- [3] Yaro, N. S. A., Napiah, M. Bin, Sutanto, M. H., Usman, A., & Saeed, S. M. (2021). Modeling and optimization of mixing parameters using response surface methodology and characterization of palm oil clinker fine modified bitumen. Construction and Building Materials, 298, 123849.
- [4] Jafri, N. H. S., Jimat, D. N., Azmin, N. F. M., Sulaiman, S., & Nor, Y. A. (2021). The potential of biomass waste in Malaysian palm oil industry: A case study of Boustead Plantation Berhad. IOP Conference Series: Materials Science and Engineering, 1192(1), 012028.
- [5] Hassan, M. A., Farid, M. A. A., Zakaria, M. R., Ariffin, H., Andou, Y., & Shirai, Y. (2024). Palm oil expansion in Malaysia and its countermeasures through policy window and biorefinery approach. *Environmental Science & Policy, 153*, 103671.
- [6] Zikri, R., Natasyah, E., & Muhdarina, M. (2022). Synthesis of oil palm fronds

- charcoal as adsorbent to reduce levels of Fe (III) in peat water. *Jurnal Kimia Sains dan Aplikasi, 25*(8), 300–306.
- [7] Sultana, M., Rownok, M. H., Sabrin, M., Rahaman, M. H., & Alam, S. M. N. (2022). A review on experimental chemically modified activated carbon to enhance dye and heavy metals adsorption. Cleaner Engineering and Technology, 6, 100382.
- [8] Gayathiri, M., Pulingam, T., Lee, K. T., & Sudesh, K. (2022). Activated carbon from biomass waste precursors: Factors affecting production and adsorption mechanism. *Chemosphere*, 294, 133764.
- [9] Jagaba, A. H., Kutty, S. R. M., Hayder, G., Baloo, L., Noor, A., Yaro, N. S. A., et al. (2021). A systematic literature review on waste-to-resource potential of palm oil clinker for sustainable engineering and environmental applications. *Materials*, 14(16), 4456.
- [10] Deraman, M., Kumar, H. S., Shamsudin, S. A., Rosli, M. I., Omar, F. S., Othman, M. A. R., et al. (2025). Effect of electrode thickness on capacitive and self-discharge performance of carbonbased supercapacitor. Key Engineering Materials, 1007, 51–62.
- [11] Natasyah, E. (2020). Sintesis dan karakterisasi karbon aktif dari limbah pelepah kelapa sawit (Elaeis guineensis Jacq.) menggunakan pengaktif kalium hidroksida [Undergraduate thesis, Universitas Riau].
- [12] Zikri, R. (2024). Sintesis komposit karbon aktif pelepah kelapa sawit—magnetit (Fe₃O₄) dengan variasi mol pengendap NaOH sebagai katalis pendegradasi metilen biru [Undergraduate thesis, Universitas Riau].
- [13] Udyani, K., & Purwaningsih, D. Y. (2021). Chemical and physical activation using a microwave to increase the ability of activated carbon to adsorb dye waste. *Journal of Physics: Conference Series*, 2117(1), 012030.
- [14] Widanarto, W., Budianti, S. I., Ghoshal, S. K., Kurniawan, C., Handoko, E., & Alaydrus, M. (2022). Improved

- microwave absorption traits of coconut shells-derived activated carbon. *Diamond and Related Materials*, 126, 109059.
- [15] Kopac, T., & Lin, S. D. (2024). A review on the characterization of microwave-induced biowaste-derived activated carbons for dye adsorption. *International Journal of Environmental Science and Technology*, 21, 8717–8748.
- [16] Duran-Jimenez, G., Rodriguez, J., Stevens, L., Altarawneh, S., Batchelor, A., Jiang, L., et al. (2024). Single-step preparation of activated carbons from pine wood, olive stones and nutshells by KOH and microwaves: Influence of ultramicroporous for high CO₂ capture. Chemical Engineering Journal, 499, 156135.
- [17] Komariyah, D. (2021). Karbonisasiaktivasi KOH/microwave pelepah kelapa sawit (Elaeis guineensis Jacq.) menjadi karbon aktif untuk mengurangi warna dan kekeruhan dalam limbah cair pabrik kelapa sawit [Undergraduate thesis, Universitas Riau].
- [18] Wahyuni, S. (2021). Karbonisasi-aktivasi KOH/microwave pelepah kelapa sawit menjadi karbon aktif untuk mengurangi TDS dari limbah cair pabrik kelapa sawit [Undergraduate thesis, Universitas Riau].
- [19] Taufik, M., Suci, T., Kasih, D., & Khair, M. (2021). Pembuatan karbon aktif cangkang kelapa sawit (Elaeis guineensis) dengan aktivator gelombang microwave. Chemistry Journal Universitas Negeri Padang, 10(1), 40– 44.
- [20] Zalmi, H., & Khair, M. (2021). Sintesis dan karakterisasi karbon aktif dari ampas tebu diaktivasi menggunakan gelombang mikro. *Jurnal Periodik Jurusan Kimia Universitas Negeri Padang, 10*(1), 38.*
- [21] Sembiring, C. H., Husnah, M., & Sirait, R. (2023). Preparasi karbon aktif limbah kulit ubi kayu menggunakan aktivasi NaOH berbantuan gelombang mikro. *Jurnal Online Fisika*, 8(1), 33–38.*
- [22] Nandi, R., Jha, M. K., Guchhait, S. K., Sutradhar, D., & Yadav, S. (2023).

- Impact of KOH activation on rice husk-derived porous activated carbon for carbon capture at flue gas alike temperatures with high CO_2/N_2 selectivity. ACS Omega, 8(6), 4802–4812 *
- [23] Purnamawati, N. (2023). Uji kualitas sintesis karbon aktif dari pelepah aren teraktivasi asam fosfat. *Journal of Research and Education in Chemistry*, 5(2), 120.*
- [24] Qodir, M. A., Alhikami, A. F., & Margianto, M. (2025). Analisis profil degradasi massa pada hydrochar menggunakan teknik hydrothermal carbonization dari limbah tandan kosong sawit. *Jurnal Teknik Mesin*, 22(1), 14–20.*
- [25] Kasandra Maidayanti, K. (2021). Efektivitas arang aktif dari limbah tatal karet sebagai media filtrasi untuk penurunan parameter pH, warna dan zat organik pada air gambut [Undergraduate thesis].
- [26] Debbache, H., Amor, A. A., Amor, F. Z. A., Khiari, R., Moussaoui, Y., Belfar, M. L., et al. (2024). A comprehensive analysis of the use of chemical technology to produce activation activated from agricultural carbon residues. Cellulose Chemistry and Technology, 58(9-10), 1149-1161.
- [27] Awitdrus, Siregar, G. M. G., Agustino, Saktioto, Iwantono, Syahputra, R. F., et al. (2021). KOH activation with microwave irradiation and its effect on the physical properties of orange peel activated carbon. *Journal of Physics: Conference Series*, 2049(1), 012025.*
- [28] Fajri, R. J. (2024). Pemanfaatan limbah kulit kopi arabika (Coffea arabica) menjadi karbon aktif sebagai adsorben zat warna metilen biru [Undergraduate thesis].
- [29] Addzikri, A. I., & Rosariawari, F. (2025). Pemanfaatan ampas tebu dan kulit pisang kepok sebagai karbon aktif pada proses adsorpsi untuk menyisihkan kadar Fe dan Mn. Jurnal Serambi Engineering, 10(1).*
- [30] Febriani, A. V., Hanum, F. F., Rahayu, A., Wardhana, B. S., & Chusna, F. M. A.

- (2025). The impact of carbonization temperature on the quality of empty fruit bunch charcoal and palm kernel charcoal for co-firing application. *Sains Natural: Jurnal Biologi dan Kimia, 15*(1), 28–39.*
- [31] Niswah, F. S., Yasa, I. W. S., & Nofrida, R. (2025). Pengaruh suhu dan lama penyangraian biji kakao terhadap karakteristik mutu teh kulit biji kakao (*Theobroma cacao* L.). *Jurnal Edukasi Pangan*, 3(1), 58–71.*
- [32] Kusniawati, E., Sari, D. K., & Putri, M. K. (2023). Pemanfaatan sekam padi sebagai karbon aktif untuk menurunkan kadar pH, turbidity, TSS, dan TDS. Journal of Innovation Research and Knowledge, 2(4), 4183–4198.*
- [33] Ayuningtias, F. S. (2023). Pemanfaatan limbah cangkang kelapa sawit (Elaeis guineensis Jacq.) menjadi arang aktif tahun 2023 [Undergraduate thesis].
- [34] Hardiansyah, M. F. (2024). Sintesis dan karakterisasi mikro-karbon dari selulosa limbah kulit ubi jalar (Ipomoea batatas) menggunakan metode microwaveassisted hydrothermal carbonization [Undergraduate thesis].
- [35] Kim, S., Lee, S.-E., Baek, S.-H., Choi, U., & Bae, H.-J. (2023). Preparation of activated carbon from Korean anthracite: Simultaneous control of ash reduction and pore development. *Processes*, 11(8), 2877.*
- [36] Ibrahim, P. P., Husain, R., & Lantu, I. S. (2025). Effect of soaking volume using pineapple peel waste vinegar on the yield, viscosity, moisture, and ash content of gelatin from tuna bone (*Thunnus* sp.). *Jurnal Ilmiah PLATAX*, 13(2), 324–334.*
- [37] Astuti, C. S., Azmi, Y., & Febrianti, F. (2024). Pembuatan arang aktif kultur jaringan dari pelepah kelapa sawit (*Elaeis guineensis* Jacq.) dengan berbagai aktivator. *Jurnal Ilmiah Respati*, 15(2), 214–225.*
- [38] Trisunaryanti, W., Triyono, T., Falah, I. I., Wicaksono, D. B., & Sumbogo, S. D. (2024). Characteristic and performance of Ni, Pt, and Pd monometal and Ni–Pd bimetal onto KOH activated carbon for

- hydrotreatment of castor oil. *Indonesian Journal of Chemistry*, 24(1), 115–124.*
- [39] Monika, I., Umar, D. F., Suganal, & Wijayanti, R. (2024). Porous structure improvement of coal activated carbon using steam activation in pilot scale. In AIP Conference Proceedings (Vol. 3003, p. 020026). AIP Publishing LLC.
- [40] Ateş, A. (2023). The effect of microwave and ultrasound activation on the characteristics of biochar produced from tea waste in the presence of H₃PO₄ and KOH. *Biomass Conversion and Biorefinery*, 13(18), 9075–9094.*
- [41] Aloud, S. S., Alharbi, H. A., Hameed, B. H., Giesy, J. P., Almady, S. S., & Alotaibi, K. D. (2023). Production of activated carbon from date palm stones by hydrothermal carbonization and microwave-assisted KOH/NaOH mixture activation for dye adsorption. *Scientific Reports*, 13, 19064. https://doi.org/10.1038/s41598-023-45641-7
- [42] Ahmad, A. A., Al-Raggad, M., Shareef, N. (2021). Production of activated carbon derived from agricultural by-products via microwaveinduced chemical activation: A review. Carbon Letters, 31(6), 957–971. https://doi.org/10.1007/s42823-021-00273-z
- [43] Adame-Pereira, M., Alexandre-Franco, M., Fernández-González, C., & Gómez-Serrano, V. (2021). Adsorption of bisphenol A by activated carbon developed from PET by KOH activation. [Journal name unavailable].
- [44] Nguyen, H. M., Tran, A. T., Nguyen, D. N. L., Lam, H. H., Tran-Thuy, T.-M., Nguyen, L. Q., et al. (2023). One-pot fabrication of zero-valent iron-embedded activated carbon from rosemary distillation residues for malachite green removal. *Materials Research Express*, 10(8), 085603.
- [45] Zikri, R., Natasyah, E., & Muhdarina, M. (2022). Synthesis of oil palm fronds charcoal as adsorbent to reduce levels of Fe (III) in peat water. *Jurnal Kimia Sains dan Aplikasi*, 25(8), 300–306.

- [46] Opoku, B. K., Isaac, A., Micheal, A. A., Bentum, J. K., & Muyoma, W. P. (2021). Characterization of chemically activated carbons produced from coconut and palm kernel shells using SEM and FTIR analyses. *American Journal of Applied Chemistry*, 9(3), 90–96.*
- [47] Wang, H., He, T., Hao, X., Huang, Y., Yao, H., Liu, F., et al. (2022). Moisture adsorption–desorption full-cycle power generation. *Nature Communications*, 13, 2524. https://doi.org/10.1038/s41467-022-30277-y
- [48] Kunusa, W. R., Iyabu, H., & Abdullah, R. (2021). FTIR, SEM and XRD analysis of activated carbon from sago wastes using acid modification. *Journal of Physics: Conference Series*, 1968(1), 012014.
- [49] Ateş, A. (2023). The effect of microwave and ultrasound activation on the characteristics of biochar produced from tea waste in the presence of H₃PO₄ and KOH. *Biomass Conversion and Biorefinery*, 13(18), 9075–9094.
- [50] Shuaib, M. M., Musah, M., & Mathew, J. T. (2024). Preparation and characterization of activated carbon from Africa star apple (*Chrysophyllum albidum*) seed shell. *FUDMA Journal of Science*, 8(3), 194–199.
- [51] Jawed, A., Saxena, V., & Pandey, L. M. (2020). Engineered nanomaterials and their surface functionalization for the

- removal of heavy metals: A review. Journal of Water Process Engineering, 33, 101009.
- [52] Chen, J., Li, X., Gao, L., Guo, S., & He, F. (2024). Microwave treatment of minerals and ores: Heating behaviors, applications, and future directions. *Minerals*, 14(3), 219.
- [53] Lawtae, P., & Tangsathitkulchai, C. (2021). A new approach for controlling mesoporosity in activated carbon by the consecutive process of air oxidation, thermal destruction of surface functional groups, and carbon activation (the OTA method). *Molecules*, 26(9), 2758.
- [54] Lan, D., Zhu, H., Zhang, J., Li, S., Chen, Q., Wang, C., et al. (2022). Adsorptive removal of organic dyes via porous materials for wastewater treatment in recent decades: A review on species, mechanisms, and perspectives. Chemosphere, 293, 133464.
- [55] He, H., Zhang, R., Zhang, P., Wang, P., Chen, N., Qian, B., et al. (2023). Functional carbon from nature: Biomassderived carbon materials and the recent progress of their applications. *Advanced Science*, 10(8), 2205557.
- [56] Ozcan, D. O., Hendekçi, M. C., & Ovez, B. (2024). Enhancing the adsorption capacity of organic and inorganic pollutants onto impregnated olive stonederived activated carbon. *Heliyon*, 10(9), e32792.